Determination of Nanosized Adsorbate Mass in Solution Using Mechanical Resonators: Elimination of the so Far Inseparable Liquid Contribution

N.B. When citing this work, cite the original published paper.

(article starts on next page)

Determination of Nanosized Adsorbate Mass in Solution Using Mechanical Resonators: Elimination of the So Far Inseparable Liquid Contribution

Antonius Armanious,* Björn Agnarsson, Anders Lundgren, Vladimir P. Zhdanov, and Fredrik Höök*

Read Online

ACCESS | Metrics & More | Article Recommendations | SI Supporting Information

ABSTRACT: Assumption-free mass quantification of nanofilms, nanoparticles, and (supra)molecular adsorbates in a liquid environment remains a key challenge in many branches of science. Mechanical resonators can uniquely determine the mass of essentially any adsorbate; yet, when operating in a liquid environment, the liquid dynamically coupled to the adsorbate contributes significantly to the measured response, which complicates data interpretation and impairs quantitative adsorbate mass determination. Employing the Navier−Stokes equation for liquid velocity in contact with an oscillating surface, we show that the liquid contribution for rigid systems can be eliminated by measuring the response in solutions with identical kinematic viscosity but different densities. Guided by this insight, we used

the quartz crystal microbalance (QCM), one of the most widely employed mechanical resonators, to experimentally demonstrate that the kinematic-viscosity matching can be utilized to quantify the dry mass of rigid and in many cases also nonrigid adsorbate systems, including, e.g., rigid nanoparticles, tethered biological nanoparticles (lipid vesicles), as well as highly hydrated polymeric films. For all the adsorbates, the dry mass determined using the kinematic-viscosity matching was within the uncertainty limits of the corresponding mass determined using complementary methods, i.e., QCM in air, scanning electron microscopy, surface plasmon resonance, and theoretical estimations. The same approach applied to the simultaneously measured energy dissipation made it possible to quantify the mechanical properties of the adsorbate and its attachment to the surface, as demonstrated by, for example, probing the hydrodynamic stabilization induced by nanoparticle crowding. In addition to a unique means to quantify the liquid contribution to the measured response of mechanical resonators, we also envision that the kinematic-viscosity-matching approach will open up applications beyond mass determination, including a new means to investigate orientation, spatial distribution, and binding strength of adsorbates without the need for complementary techniques.
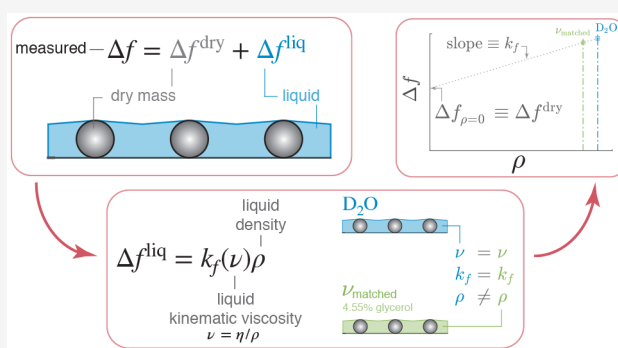
INTRODUCTION

Mass determination of nanosized adsorbates at solid−air and solid−liquid interfaces is central in many branches of science. Mechanical resonators are unique in their capacity to determine the mass of essentially any type of adsorbate at any surface without *a priori* knowledge of their physicochemical properties. In vacuum and in air, this is possible due to a direct proportionality between the measured changes in resonance frequency, Δf, and the adsorbed mass per unit area, Δm. For the quartz crystal microbalance (QCM), which is the most widely used mechanical resonator, this relationship is known as the Sauerbrey equation:[1]

$$\Delta m = -C_Q \cdot \Delta f_n / n \qquad (1)$$

where n is the overtone number and C_Q is the mass sensitivity constant, which for a 5 MHz crystal is 18 ng·Hz^{-1}·cm^{-2} (ref 2). QCM as well as many other mechanical resonators[3−5] can also operate in a liquid environment and be further extended to simultaneously monitor both Δf_n and changes in energy dissipation, ΔD_n.[6,7] However, when operated in a liquid environment, not only the adsorbate but also the surrounding liquid becomes dynamically coupled to the oscillating crystal,[8] a feature that is shared by all mechanical resonators operating in liquid. While this can in principle provide unique information about the physicochemical properties of an adsorbate, deconvoluting the entangled information in the measured response is an unresolved analytical challenge, as the measured response in a liquid environment is, in a complex manner, dependent on the mass of the adsorbate and the
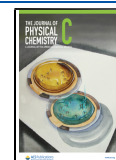
dynamically coupled liquid—a dependence that is manifested through changes in both Δf_n and ΔD_n of the resonator.[9]

Still, the rich information contained in combined Δf_n and ΔD_n measurements, especially when complemented with theoretical models representing the response for viscoelastic films,[10−12] has turned out to be very valuable in multiple research areas, including hydration analysis of organic polymers,[13,14] proteins,[15] and biological membranes.[15,16] QCM has also been widely applied to monitor and characterize thin films, including porosity determination,[17,18] monitoring the growth of mesoporous materials,[19] probing responsiveness of polymeric coatings,[20] and characterization of biomimetic membranes.[21,22] Additionally, QCM has been extensively employed to study discrete adsorbates such as abiotic and biological macromolecules and nanoparticles (NPs). These studies included investigations of biomolecular interactions of proteins[23,24] and viruses;[25,26] structure,[27,28] confirmation[29,30] and orientation changes[31] of biomacromolecules; spatial distribution,[32] size,[33−35] deformation[36,37] and dissolution[38] of NPs; protein corona formation on amyloids;[39] interactions between NPs and biomimetic membranes;[40,41] as well as bioanalytical sensor development.[42−46]

Yet, the inseparable nature of the adsorbate and liquid contributions to the measured response puts a significant limitation on quantitative interpretation of adsorption measurements in a liquid environment. In particular, this shortcoming makes mass determination using mechanical resonators nonconclusive, unless complementary methods, such as surface plasmon resonance (SPR), ellipsometry, and/or atomic force microscopy (AFM) are employed in parallel.[18,47−49]

The use of combined experimental setups, e.g., QCM/SPR or QCM/AFM, comes with many challenges, such as operation at different spatial scales, requirement for very complex setups that are inaccessible for most users, and/or the need for pretreatment procedures that tend to change the properties of the samples under investigation. Moreover, mass determination using these complementary methods requires accurate knowledge, or determination, of the physical properties of adsorbates, such as refractive index or density. Accordingly, there has in recent years been an intense, albeit so far unsuccessful, search for a means to separate the contribution of coupled liquid using QCM measurements alone.[2] Such a self-sufficient approach would obviate the need for complementary methods and provide quantitative information about the adsorbed dry mass and the coupled liquid contribution, as well as information about the dissipative energy loss associated with the adsorbate.

We here address this challenge through insights gained from the fundamental fluid dynamics principles of the Navier−Stokes equation for liquid velocity in contact with an oscillating surface[50] to show that the elimination of the liquid contribution to the sensed mass is possible by measuring the response in solutions with identical kinematic viscosity but different densities. To experimentally explore this insight, we used a QCM to investigate whether the kinematic-viscosity-matching approach can be used to eliminate the liquid contribution and thus accurately determine the dry mass for a range of different nanosized adsorbates, including inorganic rigid nanoparticles (over a broad surface-coverage range), soft biological nanoparticles (lipid vesicles), and highly hydrated polymeric films. Comparisons with complementary dry-mass determination using the QCM operated in air as well as

scanning electron microscopy (SEM), surface plasmon resonance (SPR), and theoretical predictions demonstrate excellent agreements, thus suggesting that the approach may offer a self-sufficient means to quantify the liquid contribution to the measured response of mechanical resonators enabling mass determination without the need for complementary techniques.

■ METHODS

Chemicals and Materials. Ethanol (≥99.5%) was purchased from Solveco (Roserberg, Sweden). Sodium dodecyl sulfate (SDS; ≥ 99.0%), anhydrous methanol (99.8%), glycerol (≥99%), D_2O (99.9 atom % D), DCl (≥99 atom % D), NaOD (40%wt.), HCl (1 M), NaCl (≥99%), $CaCl_2$ anhydrous (≥93%), phosphate buffered saline (PBS) tablets, bis(2-hydroxyethyl)amino-tris-(hydroxymethyl)-methane (Bis-Tris; ≥98%), citric acid monohydrate (≥98%), trisodium citrate dihydrate, poly-L-lysine (PLL; MW = 70 000−150 000), humic acids (HA), (3-aminopropyl)-dimethylethoxysilane (97%), 150 nm SiO_2 nanoparticles (NPs), anhydrous chloroform (≥99%), 1-palmitoyl-2-oleoyl-glycero-3-phosphocholine (POPC), gold(III) chloride hydrate ($HAuCl_4·xH_2O$, 99.999%), hydroquinone (≥99%), O-(2-carboxyethyl)-O'-(2-mercaptoethyl)heptaethylene glycol (>95%; MW = 458.6 Da; 500 PEG), and 2100 Da poly(ethylene glycol) 2-mercaptoethyl ether acetic acid (2000 PEG) were purchased from Merck Sigma-Aldrich (Darmstadt, Germany). 5000 Da alfa-carboxy-beta-mercapto-PEG (5000 PEG) was purchased from RAPP Polymere GmbH (Tübingen, Germany). The following cholesteryl-TEG modified DNA oligonucleotides were purchased from Eurogentec (Seraing, Belgium).

- 5′-TGG-ACA-TCA-GAA-ATA-AGG-CAC-GAC-GGA-CCC-3′-TEG-cholesterol (ssA)
- Cholesterol-TEG-5′-CCC-TCC-GTC-GTG-CCT-3′ (ssB)
- 5′-TAT-TTC-TGA-TGT-CCA-AGC-CAC-GAG-TTC−CCC-3′-TEG-cholesterol (ssC)
- Cholesterol-TEG-5′-CCC-GAA-CTC-GTG-GCT-3′ (ssD)

Buffers. Four different buffers were used:

- pH (pD) = 7.0, 150 mM NaCl, and 10 mM Bis-Tris;
- pH (pD) = 7.0, 150 mM NaCl, 2.5 mM $CaCl_2$, and 10 mM Bis-Tris;
- pH (pD) = 4.0, ≈ 3.8 mM trisodium citrate dihydrate and ≈6.2 mM citric acid monohydrate;
- PBS buffer pH (pD) = 7.4, 2.7 mM KCl, 137 mM NaCl, and 10 mM phosphate.

Buffers were prepared in

- H_2O (Milli-Q purity with resistivity ≈18.2 Ω·cm; Merck Millipore, Molsheim, France);
- 100%, 80%, 60%, and 40% of D_2O in H_2O corresponding to a molar fraction of D_2O, x_{D_2O} = 1.0, 0.8, 0.6, and 0.4, respectively;
- 4.55 wt %, 3.80 wt %, 2.99 wt %, and 2.12 wt % of glycerol in H_2O, which match the kinematic viscosity, ν, of 100%, 80%, 60%, and 40% D_2O solutions, respectively;
- 10.86 wt % of glycerol in H_2O, which match the product of the density and viscosity, $\rho\eta$, of 100% D_2O.

The physical properties of all these solutions can be found in Table S1 in the Supporting Information.

The pH of buffers in H_2O and glycerol/H_2O mixtures were determined using a Mettler-Toledo (Ohaio, US) pH meter. The pH (pD) for D_2O-containing buffers were determined using pH paper, the color of which was compared and matched against the color of a similar pH paper after submerging in the corresponding H_2O-based buffer. This procedure was followed to make sure that the buffers prepared in H_2O, D_2O, D_2O/ H_2O mixtures, or glycerol/H_2O mixtures had the same pH (pD). Note that buffer dissociation constants depend on the chemical environment so the buffer will behave differently in H_2O than in a glycerol/H_2O mixture. For this reason, adding equal amounts of the chemicals does not guarantee having the same pH; it is therefore necessary to check and adjust the pH of each solution.

H_2O-based buffers were sterilized either by autoclaving at 120 °C for 20 min or by sterile filtration using 0.22 μm Stericup-GV sterile vacuum filters (Millipore, France); all other buffers were sterile filtered using 0.22 μm Stericup-GV sterile vacuum filters (Millipore, France). Note that the buffers filtered through the 0.22 μm Stericup-GV sterile vacuum filters caused aggregation of the SiO_2 NPs, suggesting that the filter membrane released leachate in the buffer. This problem was addressed by either prewashing the filters with buffer or autoclaving the buffers instead of filtering them; the latter was only done for H_2O-based buffers.

Gold Nanoparticles Synthesis. Gold nanoparticles (Au NPs) were synthesized and surface-modified with acid-terminated poly(ethylene) glycol (PEG) with different molecular weights following the procedure outlined by Perrault and Chan.[51] A seed solution of small Au NPs were made by quickly heating a 100 mL water solution containing 0.01% (w/ v) of $HAuCl_4$. Once boiling, the solution was kept under vigorous stirring whereupon 3 mL of 1% (w/v) sodium citrate solution was quickly added. The mixture was allowed to continue to boil for 10 min developing a ruby-red color. To make Au NPs with a diameter of approximately 100 nm, a 100 mL water solution containing 0.025% (w/v) $HAuCl_4$ was mixed with 0.8 mL of seed solution. The mixture was rapidly stirred at room temperature whereupon 550 μL of 1% (w/v) sodium citrate solution was immediately added followed by 2.5 mL of a 30 mM hydroquinone solution. The solution was continuously stirred for another 60 min until its color had stabilized, indicating that the reaction was completed. The size of the Au NPs was determined using AFM to be ~70 nm in diameter. The Au NP concentration was calculated from the particle size and the amount of gold added to the synthesis assuming that all gold was consumed during the reaction.

Au NPs were surface modified by the reaction with acid-terminated PEG-thiols with a molecular weight of 458.6 Da O-(2-carboxyethyl)-O'-(2-mercaptoethyl)heptaethylene glycol, 2100 Da poly(ethylene glycol) 2-mercaptoethyl ether acetic acid or 5000 Da alfa-carboxy-beta-mercapto-PEG. On the basis of the Au NP size and concentration, the total surface area of the particles in the solution was calculated. Prior to surface modification, the Au NPs were concentrated 10 times by centrifugation (1000g, 20 min) and dilution of the obtained pellet in Milli-Q water. The concentrated Au NPs were mixed with the different thiol-PEG molecules to reach a final concentration of approximately 10 PEG molecules per nm² available Au NP surface area. The mixtures were incubated overnight whereupon the PEG-modfied Au NPs were

separated from unbound thiol-PEG and salts by four repeated runs through centrifuge filter columns with 300 kDa cutoff (PALL Nanosep Omega 300k). After the final washing step, Au NPs were kept as a concentrated stock solution until use.

POPC Vesicles Preparation. POPC was dissolved in chloroform and dried in a 50 mL round flask under vacuum at 60 °C using a rotavap setup. The dried lipids were left under vacuum overnight to get rid of any residual chloroform. The formed POPC lipid film was then rehydrated in H_2O-based buffer to a concentration of 1 mg·mL^{-1}, followed by a very brief bath sonication to dissolve any small traces of lipids off the walls of the flask. The POPC solution underwent five freeze/thawing cycles, and after which, the sample was extruded 31 times through 30 nm polycarbonate membranes (Whatman, UK) using a mini-extruder (Avanti, USA). The size of the vesicles was finally determined using dynamic light scattering (DLS) on Zetasizer Nano ZS (Malvern Panalytical, UK).

DNA Tethers Preparation. A 45-base pair DNA tether decorated with cholesterol anchors was prepared by mixing the different oligonucleotides (ssA, ssB, ssC, and ssD) as detailed hereafter. A total of 800 μL of 10 μM ssA was mixed with ssB (AB), as well as ssC with ssD (CD). The mixtures were vortexed and left to hybridize for at least 30 min at 4 °C. Afterward, the AB and CD segments were mixed together by vortexing and left to hybridize for at least 30 min at 4 °C. The ABCD dsDNA was diluted in PBS to a final concentration of 0.5 μM.

QCM Experiments. The QCM experiments were conducted in an E4 system (Biolin, Sweden) coupled to a GX-274 autosampler (Gillson, USA) on AT-cut 5 MHz quartz sensors, coated with SiO_2. The sensors were either used without modification or after silanization with amine-terminated silanes. Bare sensors were cleaned by bath sonication for 15 min in 2 wt %. SDS solution, followed by rinsing with Milli-Q water, then drying under an N_2 flow, and finally treating with O_2 plasma for 3 min directly before use. The temperature and flow rate were kept constant all through the QCM experiments at 25 °C and 50 μL·min^{-1}, respectively. At the end of the Au and SiO_2 NPs adsorption experiments, the solution in contact with the sensor was exchanged with ethanol ≥99.5%, and then the sensors were dried *in situ* under an N_2 flow and at a temperature of 60 °C; finally, the temperature was lowered again to 25 °C. This procedure was followed to dry the sensors for determining the response after drying (in air) and for further analysis using AFM and SEM while minimizing any drying effects, such as aggregation of the NPs on the surface. Step-by-step experimental and calculation procedures are presented in sections S3 and S4 in the Supporting Information.

Silanization of SiO_2 Sensors. The sensors were first cleaned by bath sonication for 15 min in 2 wt % SDS solution, followed by rinsing with Milli-Q water, O_2 plasma treatment for 3 min, immersing the surface of the sensor for 30 min with 4 M H_2SO_4, thorough rinsing under flowing Milli-Q water, thorough rinsing with anhydrous methanol, and finally, drying under an N_2 flow. The sensors were then incubated in 7.5 v/v % (3-aminopropyl)-dimethylethoxysilane in anhydrous methanol for at least 30 min. Afterward, the sensors were rinsed thoroughly with anhydrous methanol to avoid precipitation of the silanes, which happens in the presence of water or ethanol. Finally, the sensors were rinsed with Milli-Q water and mounted in the instrument for use.

Atomic Force Microscopy (AFM). A Bruker Dimension 3100 scanning probe microscopy system was used for *ex-situ* atomic force imaging of the surface of the dried QCM sensors. The height (z-distance) of both SiO_2 and Au NPs were used to determine their size. Detailed experimental and computation procedures are presented in section S5 in the Supporting Information.

Scanning Electron Microscopy (SEM). Scanning electron microscopy (Zeiss Ultra 55 FEG, in-lens mode, ETH = 2 kV) was used for general *ex-situ* characterization of the dried QCM sensor surfaces and for determination of NP surface coverage. Images were acquired at a location as close as possible to the center of the sensor; the area of the sensor which contributes the most to the QCM signal. We also tried to select an imaging area that did not show any visible drying effects, such as clear aggregation of the NPs. On the basis of the acquired images, NPs were counted using ImageJ; the total number of the NPs was then divided by the area of the image to obtain the number of NPs per μm^2. Features much larger or much smaller than the size of the NPs were not counted toward the total number of the NPs. Features which showed a double layer of NPs were double counted. Examples of these different cases, as well as detailed experimental and computation procedures, are presented in section S5 in the Supporting Information.

Surface Resonance Plasmon (SPR) Experiments. The SPR experiments were conducted using a dual wavelength, 670 and 785 nm, multiparametric SPR Navi420A (BioNavis, Finland) on silica-coated sensors. The sensors were cleaned by bath sonication for 15 min in 2 wt %. SDS solution, followed by rinsing with Milli-Q water, then drying under an N_2 flow, and finally treating in a UV/ozone chamber for 45 min directly before use. The temperature and flow rate were kept constant at 25 °C and 7 $\mu L \cdot min^{-1}$, respectively.

■ RESULTS AND DISCUSSION

For QCM, as well as many mechanical resonators, the Navier–Stokes equation describing the coupled liquid can be reduced to one of the general textbook equations (see section S1 in the Supporting Information for detailed discussion),

$$\frac{\partial}{\partial t}(\text{curl } \mathbf{v}) = \nu \Delta(\text{curl } \mathbf{v}) \tag{2}$$

where $\mathbf{v}$ is the liquid velocity and $\nu \equiv \eta/\rho$ is the liquid kinematic viscosity (η and ρ are the viscosity and density of the liquid). For firmly bound rigid adsorbates or for adsorbates with appreciably larger inertia than that of the adjacent liquid, the frequency induced by the dry mass of the adsorbate, Δf^{dry}, and the liquid-related change in frequency, Δf^{liq}, are additive. For such systems, the corresponding no-slip boundary condition at the surface– and adsorbate–liquid interface (i.e., the condition stating that the liquid velocity at the interface is the same as that of the sensor surface and adsorbate) depends only on the geometry of the interface. Accordingly, the solution of eq 2, $\mathbf{v}$, depends only on ν and the interfacial geometry. Further, the liquid-related change in frequency, Δf^{liq}, is proportional to the liquid-related force acting at the surface– and adsorbate–liquid interfaces. This force can be expressed via $\mathbf{v}$ and represented as a product of ρ and a function, $F(\nu)$, which depends only on ν and the geometry. It can be done in general (section S1 in the Supporting Information), without using an explicit expression for $\mathbf{v}$. In the context of QCM, $F(\nu)$ can be designated as k_f,

which depends only on ν and the geometry as well; i.e., we have $\Delta f^{liq} = k_f \cdot \rho$, and thus, the measured frequency response, Δf, is given by

$$\Delta f_i = \Delta f^{dry} + \Delta f_i^{liq} = \Delta f^{dry} + k_f \cdot \rho_i \tag{3}$$

where i is a subscript introduced in order to specify the type of liquid in which the measurement is performed (compared to eq 1, we do not indicate n here). For the change in dissipation induced by a firmly bound adsorbate, by analogy, we obtain (section S1 in the Supporting Information)

$$\Delta D_i = \Delta D^{mech} + \Delta D_i^{liq} = \Delta D^{mech} + k_D \cdot \eta_i \tag{4}$$

where ΔD^{mech} is the term related to the mechanically dissipated energy, ΔD_i^{liq} is the liquid-related term, and k_D is the corresponding constant which depends on ν_i and the interfacial geometry.

Physically, Δf^{dry} and ΔD^{mech} are associated with the motion of the adsorbate by itself, i.e., its motion in the absence of the surrounding liquid, with $k_f \rho_i$ and $k_D \cdot \eta_i$ being the Navier–Stokes-related liquid contributions. On the basis of the adsorbate system and liquids used, Δf^{dry} and ΔD^{mech} might also include adsorbed liquid provided these liquids are not described by the Navier–Stokes equation. This distinction will be addressed in more detail when discussing the experimental results in the following sections.

If measurements are performed in one liquid alone, eqs 3 and 4 are not very helpful for practical applications because the dependence of k_f and k_D on ν and the interfacial geometry can be analytically expressed only for flat surfaces (e.g., eq 4 in ref 8). In principle, for all other cases, this dependence can be calculated numerically[37,52] or analytically.[53−56] Numerical estimations are, however, neither straightforward nor universal, whereas analytical expressions can practically be derived only by employing severe approximations, e.g., by using Brinkman's mean-field 1D equation as was previously done in order to describe the liquid-related response of the QCM for a rough surface[57] (section S1 in the Supporting Information) or some alternative approximations for specific geometries.[53−56]

Our strategy is different and generally applicable. In particular, we suggest to quantify Δf^{dry} and ΔD^{mech} by determining k_f and k_D via measurements in different solutions matched with respect to their kinematic viscosity, i.e., in solutions with identical ν_i but different ρ_i and η_i. According to eqs 3 and 4, this will allow us to exclude the contribution of coupled liquid to the QCM signal by extrapolating the measured values to $\rho = 0$ and $\eta = 0$, respectively, and thereby extract Δf^{dry} and ΔD^{mech} from the respective intercepts, without requiring any information about the geometry of the adsorbate. Above, this approach has been validated for rigid adsorbate systems. Our experiments presented below show that it is applicable and remains fairly accurate even for viscoelastic adsorbate systems, such as biological soft matter.

To experimentally evaluate the applicability of the proposed approach, we have estimated the dry mass of 150 nm SiO_2 nanoparticles (NPs) electrostatically adsorbed on a flat QCM surface at coverages, θ, ranging from 1 to 54%. We also disentangled the liquid-related contribution to ΔD from the contribution associated with the attachment between the NPs and the surface. The latter was explored to gain new insights into the postulated influence of surface crowding of NPs on the stiffness of the attachment between each NP and the surface.[52]
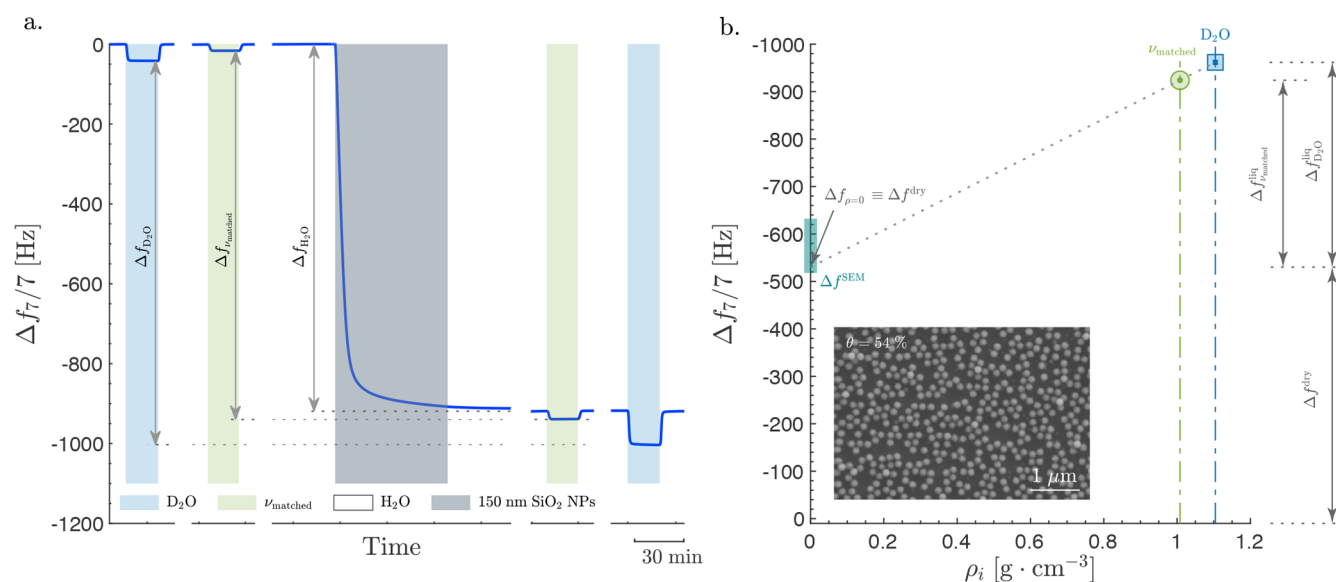
Figure 1. Experimental procedure for measuring the QCM frequency response in different solutions and disentangling the adsorbate mass and the coupled liquid mass. (a) The change in resonance frequency at the seventh overtone versus time for a flat poly-L-lysine (PLL)-coated substrate in contact with H_2O, D_2O, and a glycerol/H_2O mixture matching the kinematic viscosity of D_2O, $\nu_{matched}$; adsorption of 150 nm SiO_2 nanoparticles (NPs) until the jamming limit (corresponding to a surface coverage of 54%) is reached in an H_2O-based buffer; exchanging the solutions again to $\nu_{matched}$ and D_2O. All solutions contained 10 mM Bis-Tris, pH (pD) = 7.0, and 150 mM NaCl. Detailed experimental and calculation procedures are available in sections S2−S4 and Figures S1−S4 in the Supporting Information. (b) Frequency responses in D_2O and $\nu_{matched}$ versus liquid density and a linear extrapolation toward vanishing density. Δf^{SEM} represents the calculated frequency response based on the surface coverage determined using SEM; using a NPs size of 143 nm and a density of 2.0 ± 0.2 g·cm^{-3}. Inset shows an SEM image of the surface of the sensor after drying; scale bar = 1 μm. Detailed imaging and counting procedures for SEM are available in section S5 in the Supporting Information.

We also explored this approach for adsorption of carboxylated 70 nm gold (Au) NPs, as well as PEGylated Au NPs, to positively charged flat surfaces. For these experiments, we have varied the stiffness of the linker between the Au NPs and the surface by either varying the ionic strength of the solution or the length of the PEG linker. In addition, we tested the applicability of the approach on flexible biological NPs by assessing the dry mass of lipid vesicles tethered to the supported lipid bilayer (SLB) by DNA linkers. The similarity in structure and properties of lipid vesicles to exosomes and enveloped viruses makes them ideal models for assessing the applicability of the approach on biological nanoparticles. Finally, we extended the applicability of the approach beyond NPs by quantifying the dry mass of adsorbed humic acids (HAs), a highly hydrated[58] and permeable[59] natural polymeric material composed of supramolecular assemblies of relatively small molecules, ranging from ≃200 to 2500 Da (ref 60) with key environmental importance, due to the role they play in, among others, transport of microbes,[61] suppression of the release of greenhouse gases,[62] and photochemical oxidation of pollutants.[63]

Starting with high SiO_2 NP surface coverage (θ = 54%), Figure 1a shows the three-step kinematic-viscosity-matching procedure in which SiO_2 NPs were electrostatically adsorbed to a smooth poly-L-lysine (PLL)-coated SiO_2 sensor. After initial establishment of a baseline in buffered H_2O, the liquid in contact with the surface of the sensor was first replaced with buffered D_2O followed by a buffered glycerol/H_2O mixture (4.55 wt % glycerol) prepared to match the kinematic viscosity, $\nu = \eta/\rho$, of D_2O, henceforth referred to as $\nu_{matched}$. This was followed by adsorption of SiO_2 NPs in the H_2O-based buffer until the Δf response plateaued, after which the $\nu_{matched}$ and D_2O buffers were again subsequently injected into the flow

cell. As indicated in Figure 1a, this procedure enables measurements of the response induced upon NP adsorption in different liquids, Δf_i.

A linear extrapolation of the frequency response in D_2O, Δf_{D_2O}, and the kinematic-viscosity-matched glycerol/H_2O mixture, $\Delta f_{\nu_{matched}}$, plotted versus ρ_i (Figure 1b) yields an intercept at $\rho = 0$ of $\Delta f_{\rho=0} \approx -530$ Hz ($\equiv 9540$ ng·cm^{-2}), a value which according to eq 3 represents the frequency shift of the dry mass of the adsorbed NPs, Δf^{dry}. The obtained value is in excellent agreement with the independently determined dry mass of 10350 ± 1035 ng·cm^{-2}, based on ex-situ SEM images obtained after drying the sensor under nitrogen flow (Figure 1b, inset). Note that the liquid contribution to Δf_{H_2O}, representing the error introduced if Δf alone is used to estimate the dry mass of the adsorbate, is appreciable (≈ -390 Hz equivalent to >40% of the measured response). Further, this separation of the contributions to the measured response shows that both dry mass of the adsorbate and the mass corresponding to dynamically coupled liquid can be quantified via self-sufficient measurements using mechanical resonators alone, thus resolving a severe limitation of the technique that has for a long time disqualified its use for quantitative mass-uptake analysis in liquid environments. Although in most practical situations, adsorption measurements are carried out as in this experiment, i.e., on a flat QCM crystal already immersed in a liquid, we have, additionally, verified the applicability of the method for measurements conducted with reference to air as well as for flat surfaces without adsorbates. For flat surfaces without adsorbates, the extrapolation to $\rho = 0$ should yield $\Delta f_{\rho=0} = 0$. Indeed, the results presented in section S6 in the Supporting Information show that measurements conducted with reference to air yield the same dry mass as for
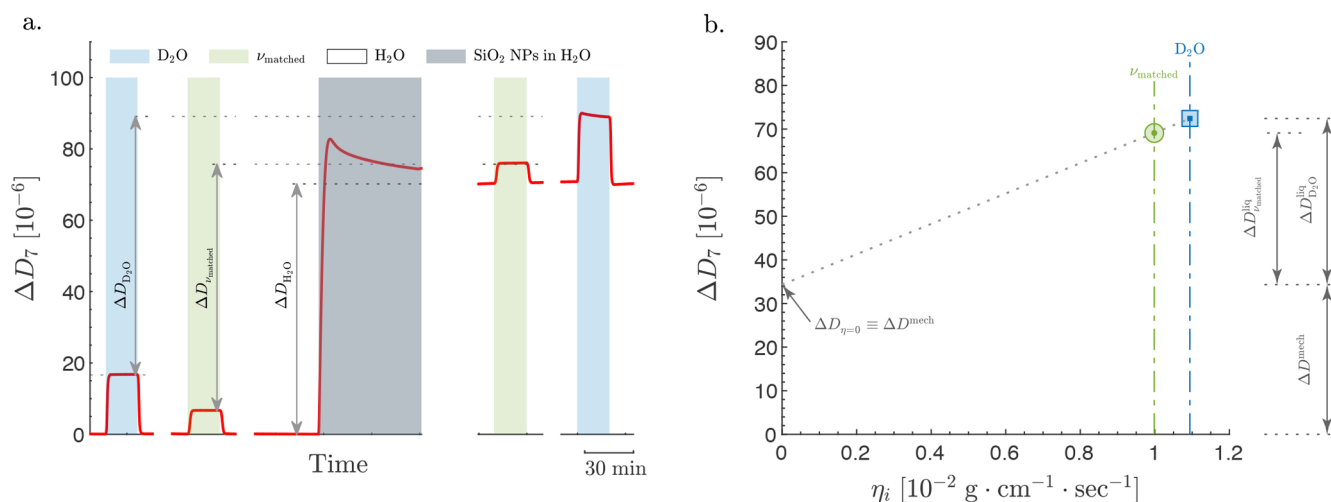
Figure 2. Experimental procedure for measuring the QCM dissipation response in different solutions and disentangling the mechanical and liquid contributions. (a) The change in dissipation at the seventh overtone versus time for a flat poly-L-lysine (PLL)-coated substrate in contact with H_2O, D_2O, and a glycerol/H_2O mixture matching the kinematic viscosity of D_2O, $\nu_{matched}$; the adsorption of 150 nm SiO_2 nanoparticles (NPs) until the jamming limit (corresponding to a surface coverage of 54%) is reached in an H_2O-based buffer; exchanging the solutions again to $\nu_{matched}$ and D_2O. All solutions contained 10 mM Bis-Tris, pH (pD) = 7.0, and 150 mM NaCl. A detailed experimental and calculation procedure is available in sections S2−S4 and Figures S1−S4 in the Supporting Information. (b) Dissipation responses in D_2O and $\nu_{matched}$ versus liquid viscosity and a linear extrapolation toward vanishing viscosity.

measurements conducted with the QCM crystal already immersed in a liquid; it also shows that for surfaces without adsorbates the extrapolated results to $\rho = 0$ yields $\Delta f_{\rho=0} \approx 0$ (at all overtones), offering additional experimental verification to the kinematic-viscosity-matching approach and also providing an internal verification for the accuracy of the preparation of the kinematic-viscosity-matched solutions by rendering an intercept at $\Delta f_{\rho=0} = 0$. As discussed in details in forthcoming sections, the extrapolation approach has been further verified using four different D_2O/H_2O mixtures and their corresponding kinematic-viscosity-matched glycerol/H_2O mixtures.

In the analysis above, the adsorbed NPs are assumed to be (i) rigid and (ii) firmly linked to the surface; i.e., the measured ΔD_i should be solely due to the liquid contribution, ΔD_i^{liq}, with no mechanically dissipated energy, $\Delta D^{mech} = 0$. For the SiO_2 NPs under consideration, assumption (i) is valid. Concerning assumption (ii), the corresponding contribution to the dissipation, ΔD^{mech}, should be zero in order for the proposed approach to be strictly valid (see eq 4). It is therefore instructive to inspect the corresponding changes in ΔD (Figure 2a) for the same sequence of injection events shown in Figure 1a.

Extrapolation of ΔD_{D_2O} and the kinematic-viscosity-matched glycerol/H_2O mixture, $\Delta D_{\nu_{matched}}$, to $\eta = 0$ has an intercept $\Delta D_{\eta=0} \approx 34 \times 10^{-6}$ (Figure 2b) which is equivalent to $-\Delta D_{\eta=0}/\Delta f_{\rho=0} = 0.06$ Hz^{-1} or 10^{-14} per NP and corresponds to ∼50% of the measured ΔD_{H_2O}. The nonzero positive $\Delta D_{\eta=0}$ was further confirmed by measurement conducted with reference to air as well as measurements of flat surfaces without adsorbate, the latter yielding $\Delta D_{\eta=0} \approx 0$ (section S6 in the Supporting Information). While $\Delta D_{\eta=0} = 0$ for the NPs would have been unequivocal evidence of rigidly adsorbed NPs, i.e., negligible viscoelastic contribution to the QCM response, this result shows that there is indeed a measurable mechanical contribution to the energy dissipation from the adsorbed NPs. For adsorbate systems with measurable viscoelastic character, $\Delta D_{\eta=0}$ does not represent the dissipated

energy under dry conditions, as in the case of perfectly rigid systems, but rather represents the mechanically dissipated energy in the adsorbate system surrounded by a liquid after excluding the energy dissipated in the liquid itself from the total dissipation response. The energy dissipated in the liquid is due to the corresponding viscous friction, which is referred to as ΔD^{liq} in this work. As a matter of fact, the dissipated energy under experimentally dry conditions, i.e., air, is in almost all cases negligible (Figure S5). $\Delta D_{\eta=0}$ in the case of rigid NPs is, thus, likely to reflect the mechanical energy dissipated due to the rotation and slippage of the NPs.[52,64] Yet, the good agreement between the independent mass determination using SEM and the dry mass obtained by extrapolating Δf_i in solutions matched with respect to the kinematic viscosity (Figure 1b) suggests that the extrapolation approach is still applicable for mass determination in spite of the positive $\Delta D_{\eta=0}$. In other words, the mechanical properties of the attachment between the NPs and the surface, reflected in a nonzero $\Delta D_{\eta=0}$, appears to have a negligible effect on $\Delta f_{\rho=0}$, thus suggesting that the kinematic-viscosity-matching approach may be applicable beyond perfectly rigid systems. We, therefore, aimed to investigate whether it is possible, using the measured QCM response only, to directly validate if the mechanical properties of the contact between a specific adsorbate and the surface have a significant influence on the dry mass determination or not.

To address this question, we performed experiments in which the stiffness of the attachment between NPs and the underlying surface was deliberately varied by replacing the PLL-coated surfaces with a surface modified with aminosilane (APDMES). Binding of NPs to the surface modified with APDMES resulted in significantly higher $\Delta D/\Delta f$ ratio than the binding to PLL did (Figure 3a), being indicative of weaker NP-surface interactions for the APDMES-modified surface (see section S7 of the Supporting Information). Furthermore, values of Δf_{H_2O} had a more pronounced overtone dependence for the APDMES-modified surface than for the PLL-coated
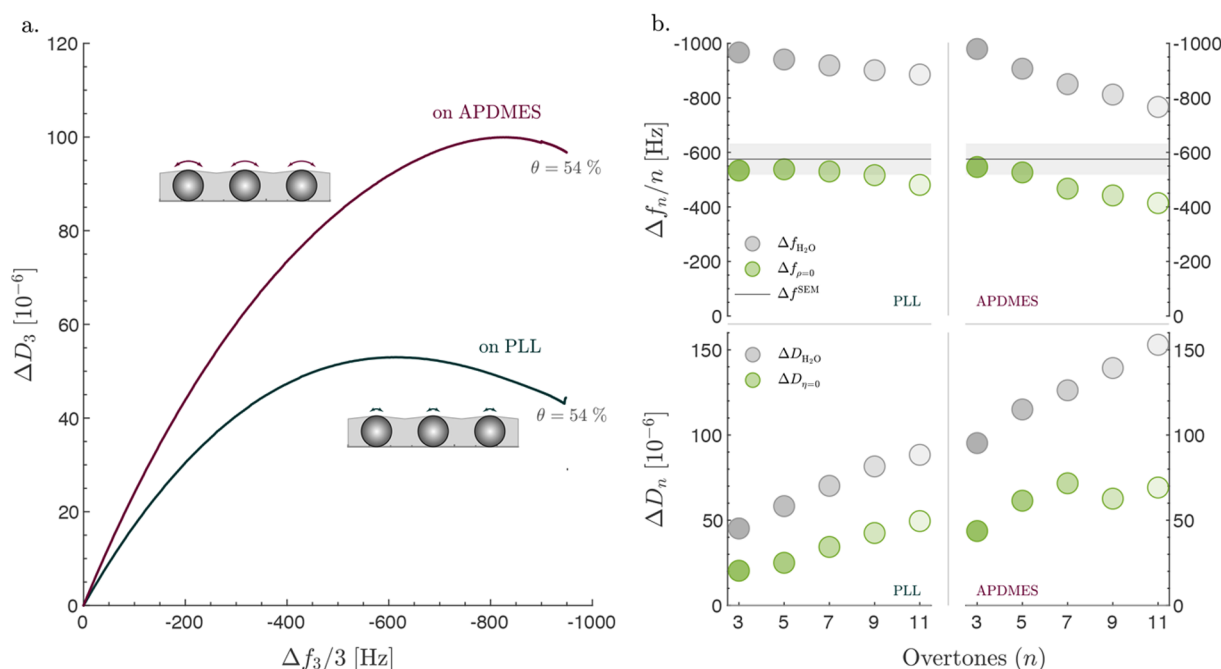
Figure 3. Effect of the flexibility of the attachment between the NPs and the substrate on dry mass determination. (a) Measured dissipation versus measured frequency at the third overtone for adsorption of 150 nm SiO_2 NPs on poly-L-lysine (PLL)-coated and on aminosilane (APDMES)-modified sensors. Two inset schematics illustrate a stronger rocking motion (represented by longer arrow on the top of each NP) for the NPs adsorbed to APDMES- than PLL-modified sensors. (b) Overtone dependence for the two experiments exhibited in panel (a), showing the measured frequency and dissipation responses in H_2O (Δf_{H_2O} and ΔD_{H_2O}) and the extrapolated frequency and dissipation responses ($\Delta f_{\rho=0}$ and $\Delta D_{\eta=0}$). Δf^{SEM} represents the calculated frequency response based on the surface coverage determined using SEM imaging; utilizing a NPs size of 143 nm and density of 2.0 ± 0.2 g·cm^{-3}. The shaded area represents the uncertainty in the Δf^{SEM} which arises from the uncertainty in the density of the NPs. All solutions contained 10 mM Bis-Tris, pH (pD) = 7.0, and 150 mM NaCl.

surface (Figure 3b, gray markers). Notably, while the overtone dependence essentially disappeared for the extrapolated $\Delta f_{\rho=0}$ for NPs bound to the PLL-coated surface, a clear overtone dependence was observed for NPs bound to the APDMES-modified surface (Figure 3b, green markers). This is expected since the adsorbate-induced $|\Delta f|$ typically decreases with increasing overtone number, n. This phenomenon arises from two different sources. The first is a viscoelastic contribution (referred to as softness in some previous work), which results in decreasing $|\Delta f|$ with increasing n.[65] The second is from an n-dependent liquid response; i.e., $|\Delta f|$ also decreases with increasing n. Notably, the n-dependent liquid response will also occur for rigidly coupled adsorbates; this has been previously shown through theoretical models[65] as well as through experimental results of rough electrodeposited copper adlayers.[66,67] Hence, for systems with a negligible viscoelastic influence on Δf, the overtone dependence of Δf will thus arise primarily from the liquid contribution, and therefore the overtone dependence is expected to vanish if the liquid contribution is eliminated using the extrapolation approach. The observed difference in the overtone dependence between APDMES and PLL for $\Delta f_{\rho=0}$ can thus be attributed to a higher viscoelastic contribution upon NP adsorption on APDMES-modified than upon PLL-coated surfaces. This conclusion is further supported by the higher ΔD_{H_2O} and $\Delta D_{\eta=0}$ values measured for the APDMES-coated surface where both the value of $\Delta D_{\eta=0}$ and the deviation between $\Delta f_{\rho=0}$ and the dry mass determined using SEM decrease with decreasing n (Figure 3b), suggesting a weaker contribution from viscoelastic losses to $\Delta f_{\rho=0}$ at lower n. In fact, the dry mass of NPs

adsorbed to the APDMES-modified surface determined from $\Delta f_{\rho=0}$ at $n = 3$ agreed perfectly with the SEM-determined value, within the uncertainty limits of the SEM approach. The overtone dependence on the linker stiffness has been further verified using two sets of experiments: (i) carboxylated Au NPs on APDMES at different ionic strengths (Figure S13) and (ii) PEGylated Au NPs with different PEG linker lengths on APDMES (Figure S13). These experiments clearly demonstrate the increasing overtone dependence of the measured and extrapolated frequency response with decreasing linker stiffness. It also shows that for all the experiments, even for Au NPs with 5000 Da PEG linker, the extrapolated frequency response at $n = 3$ accurately estimates the dry mass of the NPs within less than 10% error compared to the complementary measurements of QCM in air.

An additional long-standing question is to what extent QCM data reflect lateral interactions between closely packed adsorbates on a surface. In particular, as seen in Figures 2a and 3a, ΔD reaches a transient maximum (peak) and starts decreasing again as more NPs adsorb. This transient peak has been previously ascribed to hydrodynamic stabilization of NPs, i.e., less rotation and slippage, that becomes appreciable when NPs are sufficiently close to each other,[52] i.e., at high-enough surface coverage. We were thus curious to inspect whether the kinematic-viscosity-matching approach applied for a varying surface coverage (θ) of NPs could contribute new insight into this issue. Both the dry mass of NPs, $\Delta m_{\rho=0}$, and the mechanically dissipated energy associated with the contact zone between NPs and the surface, $\Delta D_{\eta=0}$, were therefore determined at various surface coverages, θ, ranging from 1 to 54%, (Figure 4a,c). The mass determined using the
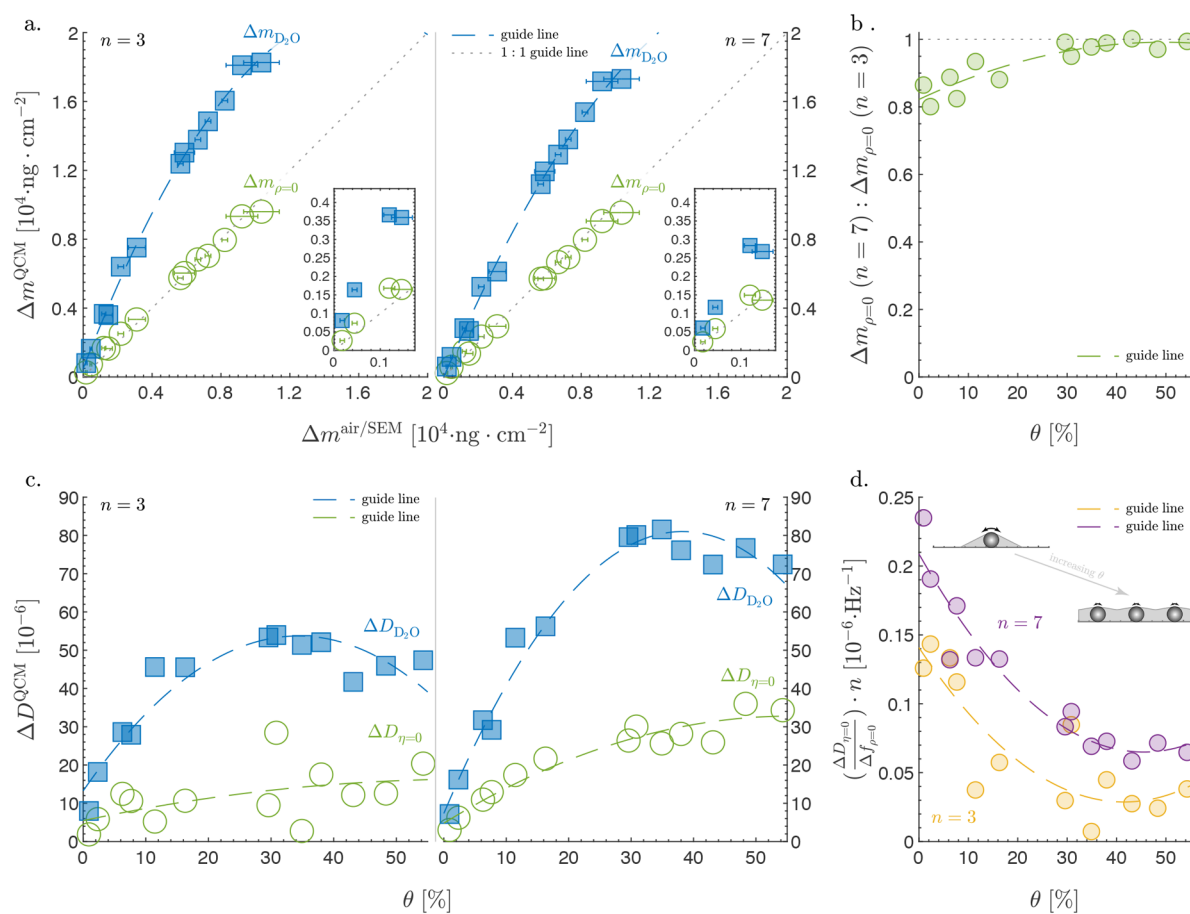
Figure 4. Disentangling the liquid and adsorbate mass/mechanical contributions to the QCM response of adsorbed SiO_2 nanoparticles over a broad range of surface coverages. (a) Comparison between the measured QCM mass in D_2O, Δm_{D_2O}, and the mass obtained by extrapolating the responses in D_2O and in a glycerol/H_2O mixture matching the kinematic viscosity of D_2O, $\nu_{matched}$, to $\rho = 0$, $\Delta m_{\rho=0}$, versus the mass determined using SEM imaging or frequency response in air. Error bars represent the uncertainty in the air or SEM measurements as detailed in section S5 in the Supporting Information. The QCM mass was calculated using the Sauerbrey equation for 5 MHz sensors: $\Delta m = -18.0 \cdot \Delta f$. Results are shown for the third and seventh overtone ($n = 3$ and 7); results from all overtones are presented in Figure S16. Insets show a zoomed-in portion of the plot in the low adsorbed mass region. (b) Ratio of the mass determined using the results of the seventh overtone to that of the third overtone versus surface coverage, θ. The surface coverages were calculated based on the SEM images or the QCM response in air. (c) Comparison between the measured QCM energy dissipation in D_2O, ΔD_{D_2O}, and the mechanically dissipated energy obtained by extrapolating the responses in D_2O and in $\nu_{matched}$ to $\eta = 0$, $\Delta D_{\eta=0}$, versus the surface coverage. Results are shown for the third and seventh overtone; results from all overtones are given in Figure S17. (d) Mechanical energy dissipated normalized by the frequency response of the dry mass for the NPs versus surface coverage at the third and seventh overtone. Inset shows a schematic illustrating a weaker rocking motion and thus less mechanically dissipated energy per particle at high surface coverage than low surface coverage. The length of the arrows on the top of NPs represents the strength of the rocking motion, which reflects the mechanically dissipated energy. All solutions contained 10 mM Bis-Tris, pH (pD) = 7, and 150 mM NaCl.

extrapolation approach, $\Delta m_{\rho=0}$ calculated based on $\Delta f_{\rho=0}$ using eq 1, and the mass determined using QCM in air or SEM, $\Delta m^{air/SEM}$, are indeed in almost perfect agreement over the entire coverage regime (Figure 4a). The overtone dependence of $\Delta m_{\rho=0}$ was fairly weak: the ratio between the seventh to the third overtone values of $\Delta m_{\rho=0}$ ranged from ~80% at the lowest coverage to higher than 95% above 30% coverage (Figure 4a,b), demonstrating that the kinematic-viscosity approach can be used to successfully disentangle the dry and liquid mass in a broad coverage regime. Further, the transient peak in the measured energy dissipation, ΔD_{D_2O}, disappears in the corresponding curve for the extrapolated $\Delta D_{\eta=0}$ (Figure 4c), revealing that the changes in liquid-related energy dissipation versus surface coverage is the source of the observed transient peak in the measured dissipation. We also observed that $\Delta D_{\eta=0}$ contributes only between 30 and 50% to

the measured dissipation at all surface coverages; i.e., the larger part of the dissipated energy is liquid-related in nature. Additionally, the contribution from the mechanically dissipated energy normalized by the extrapolated frequency response, $\Delta D_{\eta=0}/\Delta f_{\rho=0}$, decreases with increasing θ (Figure 4d), demonstrating that the mechanical energy dissipated per NP decreases with increasing θ. These observations show that the NPs are indeed mechanically stabilized with increasing θ, in good agreement with previous finite element modeling (FEM) of similar systems,[52] a conclusion also confirmed by the observed decrease in overtone dependence of $\Delta f_{\rho=0}$ with increasing θ (Figure 4b). This analysis thus shows that the kinematic-viscosity-matching approach can be used not only to accurately determine the dry mass of the adsorbate over a broad coverage range but also to experimentally quantify the mechanically dissipated energy, opening up an new avenue to access various material and/or linker properties.
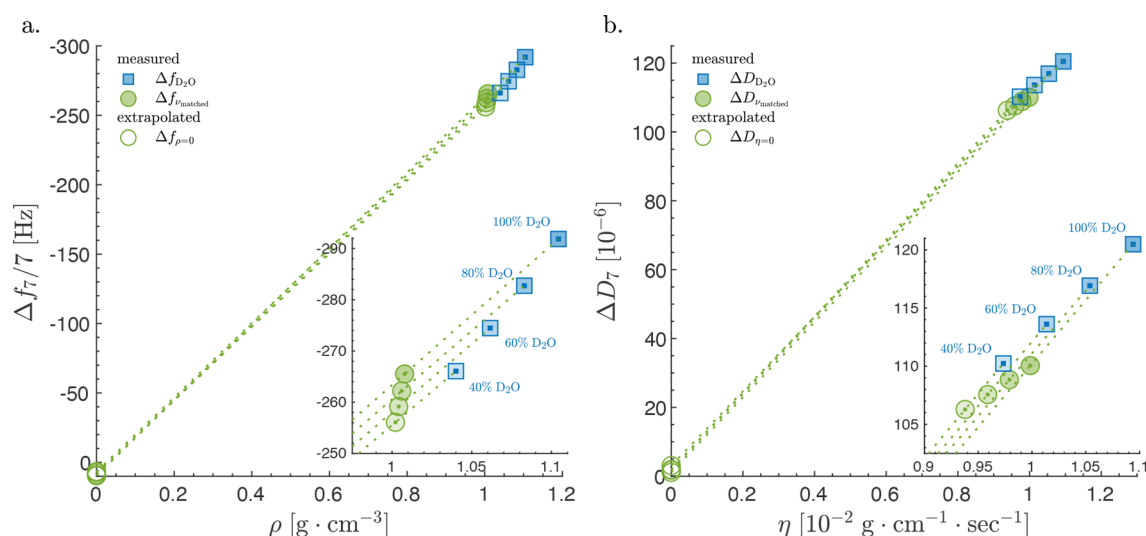
Figure 5. Extrapolation from different D_2O/H_2O mixtures and their kinematic-viscosity-matched glycerol/H_2O mixtures. (a) Frequency versus liquid density and (b) dissipation versus liquid viscosity of four different D_2O/H_2O mixtures and their kinematic-viscosity-matched glycerol/H_2O mixtures. The responses represent exchanging the medium in contact with a flat substrate from air to the different liquids. Shown as well are the extrapolation lines to $\rho = 0$ and $\eta = 0$. 100%, 80%, 60%, and 40% D_2O correspond to the molar fractions 1.0, 0.8, 0.6, and 0.4 of D_2O. Results were obtained from measurements on an aminosilane-modified sensor using a citrate-based buffer, pH (pD) = 4.0. Average results from 10 replicas and the corresponding standard deviations are shown in Figures S11 and S18 in the Supporting Information.

So far, we have relied on complementary methods, i.e., QCM in air and SEM, to verify the accuracy of the extrapolation approach. The objective of this work is to obtain accurate, trustworthy results while obviating the need for any complementary methods. As for any other scientific method, obtaining reliable data can only be achieved by conducting replicas and assessing the variability from one measurement to another. However, in some cases, it is very challenging to reproduce the same exact experimental conditions and thus outcome, such as for example, the same exact surface coverage of an adsorbate. By using more than one D_2O/H_2O mixture and their matched H_2O/glycerol mixture to estimate the dry mass and mechanical properties, one can extend the kinematic-viscosity-matching approach to provide additional confidence to the results obtained from a single measurement. Figure 5 shows the responses measured upon exchanging the medium in contact with a flat substrate from air to four different D_2O/H_2O mixtures and their corresponding kinematic-viscosity-matched glycerol/H_2O mixtures. Since there is no adsorption taking place in this process, the dry mass and the mechanical dissipated energy should be zero. Indeed, Figure 5 shows that the extrapolation from the four different pairs of kinematic-viscosity-matched solutions yields $\Delta f_{\rho=0} \approx 0$ and $\Delta D_{\eta=0} \approx 0$. We have applied this approach for flat substrates without adsorbate (Figures 5 and S18), 150 nm SiO_2 NPs at different surface coverages (Figure S19), 70 nm Au NPs at different ionic strengths (Figure S20), and 70 nm PEGylated Au NPs with different PEG linker lengths (Figure S21). The results acquired from all these experiments show that $\Delta f_{\rho=0}$ and $\Delta D_{\eta=0}$, obtained by extrapolation of the response in four different D_2O/H_2O mixtures with their corresponding kinematic-viscosity-matched glycerol/H_2O mixtures to $\rho = 0$ and $\eta = 0$, all converge to similar values. The results showed systematic dependence for neither $\Delta f_{\rho=0}$ nor $\Delta D_{\eta=0}$ on the D_2O to H_2O mixing ratios. These results provide further verification for the kinematic-viscosity-matching approach to determine the adsorbate mass and the mechanical properties of the adsorbate/surface interactions and verify the accuracy of

$\Delta f_{\rho=0}$ to determine the adsorbate mass, in agreement with the evidence provided based on the results from QCM in air and SEM imaging. This is a more crucial control in the case of $\Delta D_{\eta=0}$, because there is limited existing knowledge with respect to the nature of the mechanically dissipated energy and whether it is affected by the properties of the liquid. If there were a dependency on the liquid properties, one would have expected a systematic increase or decrease in $\Delta D_{\eta=0}$ with the increasing D_2O concentrations in the D_2O/H_2O mixtures; these results suggest that the mechanically dissipated energy was not affected by the different liquid properties within the range of liquids used in this work. Additionally, the possibility to determine $\Delta f_{\rho=0}$ and $\Delta D_{\eta=0}$ based on the extrapolation of four couples of data points provides a robust statistical verification of the analysis, especially for systems with small Δf and ΔD responses. Note that in this work we determine the dry mass and mechanically dissipated energy at down to $\theta = 1\%$ of 150 nm SiO_2 NPs, which is equivalent to $\Delta f_{\rho=0} \approx -15$ Hz and $\Delta D_{\eta=0} \approx 2 \times 10^{-6}$; -15 Hz corresponds to the mass of monolayer of small protein of ~ 5 nm in diameter at the jamming limit ($\theta = 54\%$). Finally, it is also worth noting that one could achieve a sound statistical verification of $\Delta f_{\rho=0}$ and $\Delta D_{\eta=0}$, as the one achieved using different D_2O/H_2O mixtures, by exchanging the same kinematic-viscosity-matched liquids, e.g., D_2O and 4.55 wt % glycerol in H_2O, several times before and after the adsorbate.

Encouraged by the results obtained using the kinematic-viscosity-matching approach applied on rigid NPs even under weak attachment conditions, we decided to explore the applicability of the approach to less rigid, biological NPs. As a proof of concept, we explored the possibility to determine the dry mass of POPC vesicles anchored to a supported lipid bilayer (SLB) via DNA tethers (Figure 6a,d). As previously described,[68] DNA tethers were formed of 45 base pairs with a stretched length of ~ 15 nm and have two cholesterol anchors at its ends enabling self-insertion of one end into the SLB and the other into the POPC vesicles. The flexibility of the DNA linkers and the POPC vesicles suggests that the system will
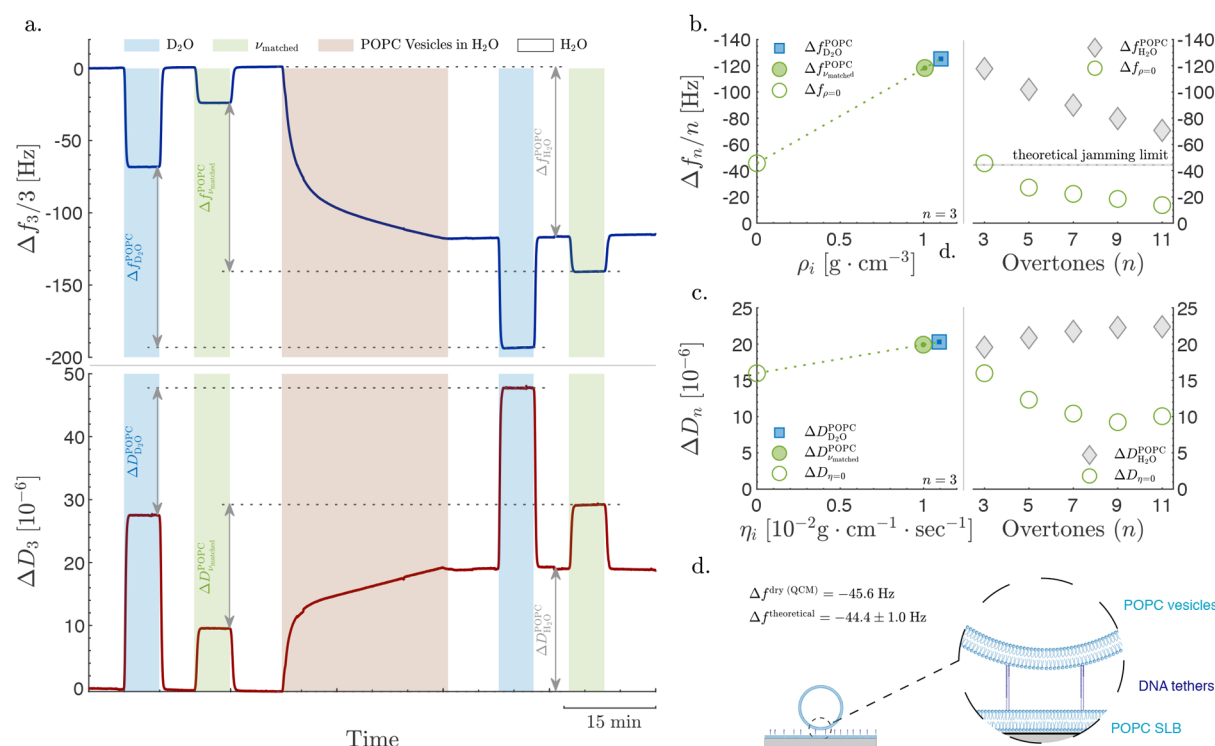
Figure 6. Disentangling the liquid and adsorbate mass/mechanical contributions to the QCM response of a tethered lipid vesicles. (a) The change in resonance frequency (upper panel) and dissipated energy (lower panel) at the third overtone versus time for the tethering of POPC lipid vesicles (size distribution shown in Figure S23) to a supported lipid bilayer (SLB) through DNA molecules with cholesterol anchors. The buffer was exchanged to a D_2O-based buffer and a glycerol/H_2O mixture matching the kinematic viscosity of D_2O, $\nu_{matched}$, before and after the POPC adsorption step. A complete experimental procedure including the formation of SLB and attachment of the DNA tethers is shown in Figure S23. (b) Frequency responses (left panel) for the POPC vesicles in D_2O and $\nu_{matched}$ versus liquid density and a linear extrapolation toward vanishing density, $\rho = 0$. Overtone dependence (right panel) for the measured frequency responses in H_2O, Δf_{H_2O}, and the extrapolated frequency responses, $\Delta f_{\rho=0}$, of the POPC vesicles. The theoretical frequency response, $\Delta f^{theoretical}$, was calculated using the Sauerbrey equation for 5 MHz sensors: $\Delta m = -18.0 \cdot \Delta f$ based on POPC molecular weight of 760.076 g·mol^{-1}, area per lipid of 0.683 ± 0.015 nm^2 (ref 69) and assumed surface coverage of $\theta = 54\%$. The shaded area represents the uncertainty in the theoretical estimation, arising from the uncertainty in the area per lipid molecule. (c) Dissipation responses (left panel) for the POPC vesicles from D_2O and $\nu_{matched}$ versus liquid viscosity and a linear extrapolation toward vanishing viscosity, $\eta = 0$. Overtone dependence (right panel) for the measured dissipation responses in H_2O, ΔD_{H_2O}, and the extrapolated dissipation, $\Delta D_{\eta=0}$, of the POPC vesicles. (d) A schematic showing POPC vesicles tethered to SLB via DNA molecules. Experimental details, characterization of vesicles, and calculations are presented in section S11 in the Supporting Information. All solutions contained 10 mM phosphate buffer, pH (pD) = 7.4, 2.7 mM KCl, and 137 mM NaCl.

have an appreciable viscoelastic character; indeed, the measured Δf_{H_2O} showed a very strong overtone dependence ranging from -120 Hz at $n = 3$ to -70 Hz at $n = 11$ (Figure 6b), and the $-\Delta D_{H_2O}/\Delta f_{H_2O}$ ratio ranged from 0.17 at $n = 3$ to 0.32 for $n = 11$ (Figure 6b,c). Extrapolation of the frequency response in D_2O and $\nu_{matched}$ buffers toward $\rho = 0$ yields an intercept $\Delta f_{\rho=0}$ of -45.6 Hz at $n = 3$ but with a strong overtone dependence (Figure 6b). $\Delta f_{\rho=0}$ at $n = 3$ is in excellent agreement with the theoretically estimated frequency response using the Sauerbrey equation (eq 1) based on the POPC molecular weight of 760.076 g ·mol^{-1}, area per lipid of 0.683 ± 0.015 nm^2 (ref 69), and surface coverage of $\theta = 54\%$. The assumed surface coverage is justified by the plateauing adsorption profile of the POPC vesicles (Figure 6a), which indicates that the surface coverage is very close to the jamming limit. Notably, the theoretical frequency response is independent of the size of the vesicles as detailed in section S11 in the Supporting Information. It is worth mentioning that $\Delta f_{\rho=0}$ determined here represents the dry mass of the lipids only in the POPC vesicles without the mass of the liquid in

their core. This is because both D_2O and glycerol are permeable to lipid membranes:[70,71] with D_2O and H_2O having permeability coefficients in the range of 10^{-3} to 10^{-2} cm·s^{-1} and glycerol in the range of 10^{-6} to 10^{-5} cm·s^{-1};[71] thus, the liquid inside the vesicles is almost instantaneously exchanged when exchanging the bulk liquid.[72] From a theoretical perspective, the liquid inside the vesicles is in this case included in the Navier−Stokes-related liquid contributions, i.e., $k_f\rho_i$ in eq 3. If one instead would use two liquids that are impermeable to the vesicles, $k_f\rho_i$ would not include the liquid inside the vesicles, and thus $\Delta f_{\rho=0}$ would represent the mass of the lipids and the liquid inside the vesicles—a distinction that is very important for correct data interpretation. Moreover, it is crucial to emphasize that determining the dry mass of the vesicles was only possible because the tethered lipid vesicles are expected to have the same structural, distribution, and binding properties in both D_2O and $\nu_{matched}$ buffers; measurable changes in the properties of the adsorbate system when exchanging between the two liquids would have resulted in different k_f and k_D values for each of the liquids and thus an inaccurate estimation of $\Delta f_{\rho=0}$ and $\Delta D_{\eta=0}$. Finally, by
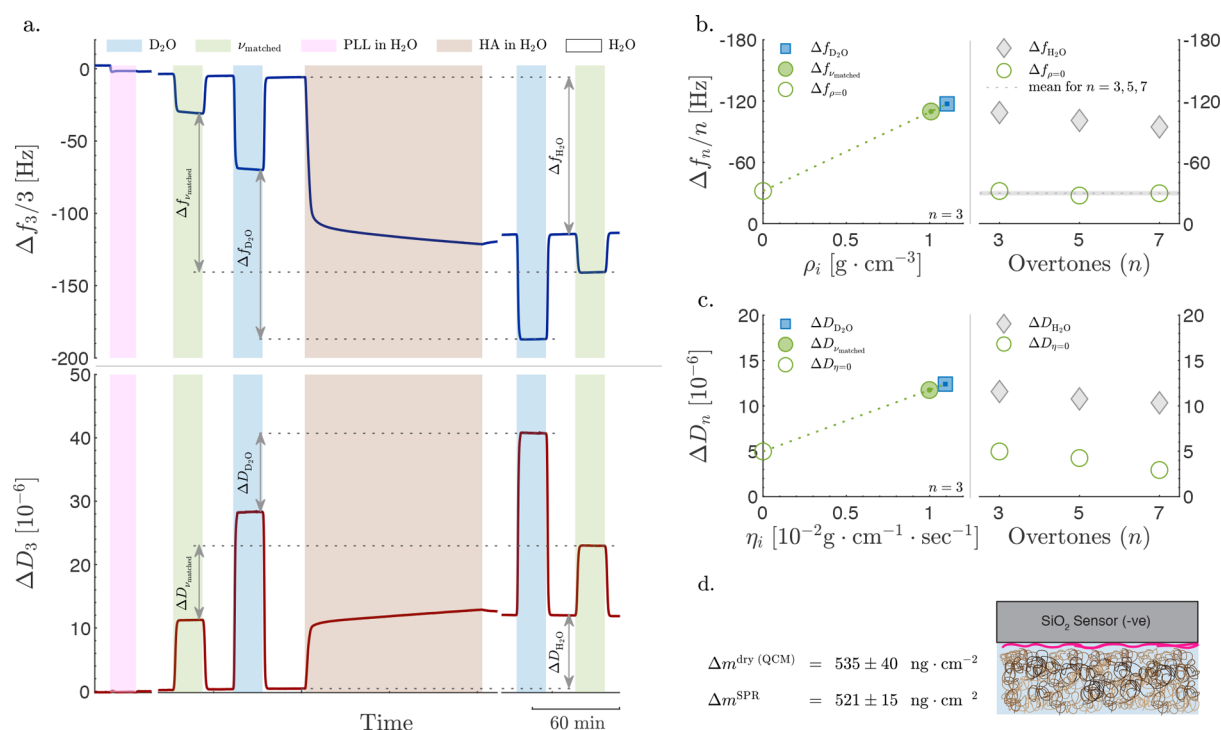
Figure 7. Disentangling the liquid and adsorbate mass/mechanical contributions to the QCM response of a polymer adlayer. (a) The change in resonance frequency (upper panel) and dissipated energy (lower panel) at the third overtone versus time for the adsorption of poly-L-lysine (PLL) adlayer on a bare SiO_2 sensor, followed by deposition of a humic acids (HA) adlayer. The buffer was exchanged to D_2O-based buffer and glycerol/H_2O mixture matching the kinematic viscosity of D_2O, $\nu_{matched}$, before and after the HA adsorption step. (b) Frequency responses (left panel) for the HA layers from D_2O and $\nu_{matched}$ versus liquid density and a linear extrapolation toward vanishing density, $\rho = 0$. Overtone dependence (right panel) for the measured frequency responses in H_2O, Δf_{H_2O}, and the extrapolated frequency responses, $\Delta f_{\rho=0}$, of the HA adlayer. Results are shown for $n = 3$, 5, and 7; results from higher overtone numbers could not be utilized due to unstable instrumental signal. The dashed line represents the mean from the three overtones, and the shaded area represents the standard deviation. (c) Dissipation responses (left panel) for the HA layers from D_2O and $\nu_{matched}$ versus liquid viscosity and a linear extrapolation toward vanishing viscosity, $\eta = 0$. Overtone dependence (right panel) for the measured dissipation responses in H_2O, ΔD_{H_2O}, and the extrapolated dissipation, $\Delta D_{\eta=0}$, of the HA adlayer. Results are shown for $n = 3$, 5, and 7; results from higher overtone numbers could not be utilized due to the unstable instrumental signal. (d) A schematic showing the HA adlayer (in brown) on the PLL (in magenta)-coated SiO_2 sensor. The dry mass, $\Delta m^{dry\,(QCM)}$, was calculated using the Sauerbrey equation for 5 MHz sensors: $\Delta m = -18.0 \cdot \Delta f$ based on $\Delta f_{\rho=0}$ averaged from $n = 3$, 5, and 7. Δm^{SPR} was determined as detailed in section S12 in the Supporting Information. All solutions contained 10 mM Bis-Tris, pH (pD) = 7.0, 150 mM NaCl, and 2.5 mM $CaCl_2$.

inspecting $\Delta D_{\eta=0}$ at $n = 3$, we observe that most of the energy dissipated is mechanical in nature, which is in agreement with the expected strong viscoelastic character of the adsorbate system. Note that $\Delta D_{\eta=0}$ not only reflects the mechanical properties of the linker, as in the cases of SiO_2 and Au NPs, but also reflects the mechanical properties of the vesicles themselves. Altogether, these results show that the kinematic-viscosity-matching approach seems capable to provide valuable information beyond rigid systems to systems with appreciable viscoelastic character.

The principles introduced above to determine the dry mass of adsorbed NPs are expected to also apply to adsorbed polymer films,[73] given that they are in a regime with sufficiently small viscoelastic contributions, i.e., where the Sauerbrey equation (eq 1) is applicable not only for the dry mass but also the liquid coupled to the adsorbed polymer. This was tested by investigating electrostatically driven adsorption of HA to a PLL-coated sensor (Figure 7a), using the aforementioned strategy of kinematic-viscosity matching. Extrapolation of the frequency response in D_2O and $\nu_{matched}$ buffers toward $\rho = 0$ yields an intercept $\Delta f_{\rho=0}$ of -29.8 ± 2.2 Hz with essentially no overtone dependence for $\Delta f_{\rho=0}$ values (Figure 7b). Additionally, conversion of $\Delta f_{\rho=0}$ into mass using

eq 1 perfectly agrees with the mass obtained by employing complementary SPR measurements (see Figure 7d and section S12 in the Supporting Information), confirming the validity of the extrapolation approach to determine the dry mass. Additionally, the mechanically dissipated energy represented by $\Delta D_{\eta=0}$ is less than half of the total dissipation, demonstrating that the majority of the dissipated energy is liquid-related in nature. For the applicability of the Sauerbrey equation on polymeric adlayers, it has been suggested that the dissipation-to-frequency ratio should be much smaller than 0.4×10^{-6} Hz^{-1}.[2] Although $\Delta D_{H_2O}/\Delta f_{H_2O}$ upon HA adsorption ($\approx 0.11 \times 10^{-6}$ Hz^{-1}) is indeed smaller than this threshold, it is on the same order and thus does not completely meet this criterion. Still, the perfect agreement of $\Delta f_{\rho=0}$ with the mass determined using SPR suggests that the kinematic-viscosity-matching approach is applicable beyond perfectly rigid systems also for polymeric adlayers as for NPs.

■ CONCLUSIONS

Taken together, our results demonstrate that the proposed kinematic-viscosity-matching approach makes it possible to determine the (dry) molecular mass of both nanoscale

adsorbates of arbitrary shape as well as polymeric adlayers, even for systems with appreciable viscoelastic contributions, and that the mechanically dissipated energy associated with the adsorbate and/or its attachment can be specifically quantified. This approach has been theoretically validated for firmly attached rigid adsorbates. While for biological soft matter the theoretical representation is far from trivial, our experiments indicate that for many such systems the approach proposed yields dry mass estimations within the uncertainty limits of the complementary methods used to verify the quantification of the adsorbed mass. More specifically, the experiments show that at lower overtones the liquid-related contribution to the QCM signal appears to be more related to the shape of soft matter (which is often rather complex) than to its deformation due to the oscillation of the crystal. The results also show that the dry-mass determination can be self-sufficiently validated based on the overtone dependence of the extrapolated $\Delta f_{\rho=0}$. For systems with weak to no measurable overtone dependence, the viscoelastic contribution is negligible, and thus the true dry mass can be determined based on any of the measured overtones. For systems with an appreciable overtone dependence, the mass determination at the lowest overtone number is the most reliable, highlighting one of the key discoveries in this work, namely, that the accuracy of the Sauerbrey equation is overtone dependent; i.e., the lower the overtone, the closer the Sauerbrey mass to the real mass. In addition, the approach does not require any *a priori* knowledge about the adsorbed material, which makes it unique in comparison with most commonly applied *in situ* methods, where ellipsometry and SPR stand out as the most reliable and commonly used. However, for accurate mass determination using these methods, at least the derivative of the refractive index with respect to the concentration of the adsorbate, dn/dc, must be known or independently determined. Additionally, in the case of SPR, also the film thickness and the decay length of the evanescent sensing field have to be determined independently. Finally, the possibility to simultaneously determine the dry mass and mechanical properties of nanosized adsorbates as well as the liquid contributions using a single method and on the same spatial scale provides a unique opportunity to potentially extract more detailed information about the adsorbates, such as investigating orientation, spatial distribution, and binding strength of adsorbates. Additionally, although demonstrated here using QCM, the kinematic-viscosity-matching approach is potentially applicable beyond the QCM to a variety of mechanical resonators that operate in a liquid environment and could thus be utilized for single cell[5] and even single virus[74] mass determination.

ASSOCIATED CONTENT

Supporting Information

The Supporting Information is available free of charge at https://pubs.acs.org/doi/10.1021/acs.jpcc.1c04502.

Detailed theoretical derivation; theoretical analysis on the applicablity of the kinematic-viscosity-matching approach on mechanical resonators other than the QCM; calculation of the physical properties of different D_2O/H_2O and glycerol/H_2O mixtures; detailed methods and experimental procedure to measure the response in different liquids and for independent mass determination using measurements in air and SEM; experimental results for measurements with reference to air, polymer adsorption to APDMES-coated sensors, adsorption of carboxylated and PEGylated Au NPs, response at different overtones and D_2O concentrations, lipid vesicles characterization and tethering, SPR calculations and results (PDF)

AUTHOR INFORMATION

Corresponding Authors

Antonius Armanious − *Division of Nano and Biological Physics, Department of Physics, Chalmers University of Technology, 41296 Gothenburg, Sweden;* Present Address: Laboratory of Food and Soft Materials, Department of Health Sciences and Technology, ETH Zürich, 8092 Zürich, Switzerland; orcid.org/0000-0002-8809-4659; Email: armanioa@ethz.ch

Fredrik Höök − *Division of Nano and Biological Physics, Department of Physics, Chalmers University of Technology, 41296 Gothenburg, Sweden;* orcid.org/0000-0003-1994-5015; Email: fredrik.hook@chalmers.se

Authors

Björn Agnarsson − *Division of Nano and Biological Physics, Department of Physics, Chalmers University of Technology, 41296 Gothenburg, Sweden;* orcid.org/0000-0003-3364-7196

Anders Lundgren − *Department of Chemistry and Molecular Biology, University of Gothenburg, 40530 Gothenburg, Sweden;* orcid.org/0000-0002-8537-9974

Vladimir P. Zhdanov − *Division of Nano and Biological Physics, Department of Physics, Chalmers University of Technology, 41296 Gothenburg, Sweden; Boreskov Institute of Catalysis, Russian Academy of Sciences, Novosibirsk 630090, Russia;* orcid.org/0000-0002-0167-8783

Complete contact information is available at:
https://pubs.acs.org/10.1021/acs.jpcc.1c04502

Author Contributions

A.A. and F.H. conceived the idea. V.P.Z. developed the theoretical formalism. A.A., B.A., and A.L. designed and performed the experiments. A.A., V.P.Z., and F.H. wrote the paper with input from all authors.

Notes

The authors declare no competing financial interest.

REFERENCES

(1) Sauerbrey, G. Verwendung von Schwingquarzen zur Wägung dünner Schichten und zur Mikrowägung. *Eur. Phys. J. A* **1959**, *155*, 206−222.

(2) Reviakine, I.; Johannsmann, D.; Richter, R. P. Hearing what you cannot see and visualizing what you hear: interpreting quartz crystal microbalance data from solvated interfaces. *Anal. Chem.* **2011**, *83*, 8838−8848.

(3) Ward, M. D.; Buttry, D. A. *In-situ* interfacial mass detection with piezoelectric transducers. *Science* **1990**, *249*, 1000−1007.

(4) Kosaka, P. M.; Pini, V.; Ruz, J. J.; Da Silva, R. A.; González, M. U.; Ramos, D.; Calleja, M.; Tamayo, J. Detection of cancer biomarkers in serum using a hybrid mechanical and optoplasmonic nanosensor. *Nat. Nanotechnol.* **2014**, *9*, 1047−1053.

(5) Martínez-Martín, D.; Fläschner, G.; Gaub, B.; Martin, S.; Newton, R.; Beerli, C.; Mercer, J.; Gerber, C.; Müller, D. J. Inertial picobalance reveals fast mass fluctuations in mammalian cells. *Nature* **2017**, *550*, 500−505.

(6) Tessier, L.; Patat, F.; Schmitt, N.; Feuillard, G.; Thompson, M. Effect of the generation of compressional waves on the response of the thickness-shear mode acoustic wave sensor in liquids. *Anal. Chem.* **1994**, *66*, 3569−3574.

(7) Rodahl, M.; Höök, F.; Krozer, A.; Brzezinski, P.; Kasemo, B. Quartz crystal microbalance setup for frequency and Q-factor measurements in gaseous and liquid environments. *Rev. Sci. Instrum.* **1995**, *66*, 3924−3930.

(8) Kanazawa, K. K.; Gordon, J. G. Frequency of quartz microbalance in contact with liquid. *Anal. Chem.* **1985**, *57*, 1770−1771.

(9) Höök, F.; Kasemo, B.; Nylander, T.; Fant, C.; Sott, K.; Elwing, H. Variations in coupled water, viscoelastic properties and film thickness of a Mefp-1 protein film during adsorption and cross-linking: a QCM-D, ellipsometry and SPR study. *Anal. Chem.* **2001**, *73*, 5796−5804.

(10) Wolff, O.; Seydel, E.; Johannsmann, D. Viscoelastic properties of thin films studied with quartz crystal resonators. *Faraday Discuss.* **1997**, *107*, 91−104.

(11) Voinova, M. V.; Rodahl, M.; Jonson, M.; Kasemo, B. Viscoelastic acoustic response of layered polymer films at fluid-solid interfaces: continuum mechanics approach. *Phys. Scr.* **1999**, *59*, 391−396.

(12) Johannsmann, D. Viscoelastic, mechanical, and dielectric measurements on complex samples with the quartz crystal microbalance. *Phys. Chem. Chem. Phys.* **2008**, *10*, 4516−4534.

(13) Arazoe, H.; Miyajima, D.; Akaike, K.; Araoka, F.; Sato, E.; Hikima, T.; Kawamoto, M.; Aida, T. An autonomous actuator driven by fluctuations in ambient humidity. *Nat. Mater.* **2016**, *15*, 1084−1089.

(14) Liu, P.; Song, M.; Zhao, T.; Gunthe, S. S.; Ham, S.; He, Y.; Qin, Y. M.; Gong, Z.; Amorim, J. C.; Bertram, A. K.; Martin, S. T. Resolving the mechanisms of hygroscopic growth and cloud condensation nuclei activity for organic particulate matter. *Nat. Commun.* **2018**, *9*, 4076.

(15) Reinisch, L.; Kaiser, R. D.; Krim, J. Measurement of protein hydration shells using a quartz microbalance. *Phys. Rev. Lett.* **1989**, *63*, 1743−1746.

(16) Fu, Y.; Jiang, Y.-B.; Dunphy, D.; Xiong, H.; Coker, E.; Chou, S. S.; Zhang, H.; Vanegas, J. M.; Croissant, J. G.; Cecchi, J. L.; Rempe, S. B.; Brinker, C. J. Ultra-thin enzymatic liquid membrane for CO_2 separation and capture. *Nat. Commun.* **2018**, *9*, 990.

(17) Feng, S.; Bein, T. Growth of oriented molecular sieve crystals on organophosphonate films. *Nature* **1994**, *368*, 834−836.

(18) Shpigel, N.; Sigalov, S.; Malchik, F.; Levi, M. D.; Girshevitz, O.; Khalfin, R. L.; Aurbach, D. Quantification of porosity in extensively nanoporous thin films in contact with gases and liquids. *Nat. Commun.* **2019**, *10*, 4394.

(19) Walcarius, A.; Sibottier, E.; Etienne, M.; Ghanbaja, J. Electrochemically assisted self-assembly of mesoporous silica thin films. *Nat. Mater.* **2007**, *6*, 602−608.

(20) Trachsel, L.; Romio, M.; Grob, B.; Zenobi-Wong, M.; Spencer, N. D.; Ramakrishna, S. N.; Benetti, E. M. Functional nanoassemblies of cyclic polymers show amplified responsiveness and enhanced protein-binding ability. *ACS Nano* **2020**, *14*, 10054−10067.

(21) Richter, R. P.; Hock, K. K.; Burkhartsmeyer, J.; Boehm, H.; Bingen, P.; Wang, G.; Steinmetz, N. F.; Evans, D. J.; Spatz, J. P. Membrane-grafted hyaluronan films: a well-defined model system of glycoconjugate cell coats. *J. Am. Chem. Soc.* **2007**, *129*, 5306−5307.

(22) Shen, H.-H.; Leyton, D. L.; Shiota, T.; Belousoff, M. J.; Noinaj, N.; Lu, J.; Holt, S. A.; Tan, K.; Selkrig, J.; Webb, C. T.; Buchanan, S. K.; Martin, L. L.; Lithgow, T. Reconstitution of a nanomachine driving the assembly of proteins into bacterial outer membranes. *Nat. Commun.* **2014**, *5*, 5078.

(23) Dubacheva, G. V.; Araya-Callis, C.; Geert Volbeda, A.; Fairhead, M.; Codée, J.; Howarth, M.; Richter, R. P. Controlling multivalent binding through surface chemistry: model study on streptavidin. *J. Am. Chem. Soc.* **2017**, *139*, 4157−4167.

(24) Gutiérrez Sánchez, C.; Su, Q.; Schönherr, H.; Grininger, M.; Nöll, G. Multi-ligand-binding flavoprotein dodecin as a key element for reversible surface modification in nano-biotechnology. *ACS Nano* **2015**, *9*, 3491−3500.

(25) Parveen, N.; Rydell, G. E.; Larson, G.; Hytönen, V. P.; Zhdanov, V. P.; Höök, F.; Block, S. Competition for membrane receptors: norovirus detachment via lectin attachment. *J. Am. Chem. Soc.* **2019**, *141*, 16303−16311.

(26) Di Iorio, D.; Verheijden, M. L.; Van Der Vries, E.; Jonkheijm, P.; Huskens, J. Weak multivalent binding of influenza hemagglutinin nanoparticles at a sialoglycan-functionalized supported lipid bilayer. *ACS Nano* **2019**, *13*, 3413−3423.

(27) Mateos-Gil, P.; Tsortos, A.; Velez, M.; Gizeli, E. Monitoring structural changes in intrinsically disordered proteins using QCM-D: Application to the bacterial cell division protein ZipA. *Chem. Commun.* **2016**, *52*, 6541−6544.

(28) Roach, P.; Farrar, D.; Perry, C. C. Interpretation of protein Adsorption: surface-induced conformational changes. *J. Am. Chem. Soc.* **2005**, *127*, 8168−8173.

(29) Tsortos, A.; Papadakis, G.; Gizeli, E. Shear acoustic wave biosensor for detecting DNA intrinsic viscosity and conformation: A study with QCM-D. *Biosens. Bioelectron.* **2008**, *24*, 836−841.

(30) Papadakis, G.; Tsortos, A.; Gizeli, E. Acoustic characterization of nanoswitch structures: Application to the DNA holliday junction. *Nano Lett.* **2010**, *10*, 5093−5097.

(31) Bisker, G.; Dong, J.; Park, H. D.; Iverson, N. M.; Ahn, J.; Nelson, J. T.; Landry, M. P.; Kruss, S.; Strano, M. S. Protein-targeted corona phase molecular recognition. *Nat. Commun.* **2016**, *7*, 1−14.

(32) Schmudde, M.; Grunewald, C.; Goroncy, C.; Noufele, C. N.; Stein, B.; Risse, T.; Graf, C. Controlling the interaction and non-close-packed arrangement of nanoparticles on large areas. *ACS Nano* **2016**, *10*, 3525−3535.

(33) Tellechea, E.; Johannsmann, D.; Steinmetz, N. F.; Richter, R. P.; Reviakine, I. Model-independent analysis of QCM data on colloidal particle adsorption. *Langmuir* **2009**, *25*, 5177−5184.

(34) Olsson, A. L.; Quevedo, I. R.; He, D.; Basnet, M.; Tufenkji, N. Using the quartz crystal microbalance with dissipation monitoring to evaluate the size of nanoparticles deposited on surfaces. *ACS Nano* **2013**, *7*, 7833−7843.

(35) Gillissen, J. J. J.; Tabaei, S. R.; Jackman, J. A.; Cho, N.-J. A model derived from hydrodynamic simulations for extracting the size of spherical particles from the quartz crystal microbalance. *Analyst* **2017**, *142*, 3370−3379.

(36) Reviakine, I.; Gallego, M.; Johannsmann, D.; Tellechea, E. Adsorbed liposome deformation studied with quartz crystal microbalance. *J. Chem. Phys.* **2012**, *136*, 084702.

(37) Gillissen, J. J. J.; Jackman, J. A.; Tabaei, S. R.; Yoon, B. K.; Cho, N.-J. Quartz crystal microbalance model for quantitatively probing the deformation of adsorbed particles at low surface coverage. *Anal. Chem.* **2017**, *89*, 11711−11718.

(38) Zou, T.; Sipponen, M. H.; Henn, A.; Österberg, M. Solvent-resistant lignin-epoxy hybrid nanoparticles for covalent surface modification and high-strength particulate adhesives. *ACS Nano* **2021**, *15*, 4811−4823.

(39) Pilkington, E. H.; Gustafsson, O. J. R.; Xing, Y.; Hernandez-Fernaud, J.; Zampronio, C.; Kakinen, A.; Faridi, A.; Ding, F.; Wilson, P.; Ke, P. C.; et al. Profiling the serum protein corona of fibrillar human islet amyloid polypeptide. *ACS Nano* **2018**, *12*, 6066−6078.

(40) Melby, E. S.; Lohse, S. E.; Park, J. E.; Vartanian, A. M.; Putans, R. A.; Abbott, H. B.; Hamers, R. J.; Murphy, C. J.; Pedersen, J. A.

Cascading effects of nanoparticle coatings: surface functionalization dictates the assemblage of complexed proteins and subsequent interaction with model cell membranes. *ACS Nano* **2017**, *11*, 5489–5499.

(41) Lochbaum, C. A.; Chew, A. K.; Zhang, X.; Rotello, V.; Van Lehn, R. C.; Pedersen, J. A. Lipophilicity of cationic ligands promotes irreversible adsorption of nanoparticles to lipid bilayers. *ACS Nano* **2021**, *15*, 6562–6572.

(42) Janshoff, A.; Galla, H. J.; Steinem, C. Piezoelectric mass-sensing devices as biosensors - An alternative to optical biosensors? *Angew. Chem., Int. Ed.* **2000**, *39*, 4004–4032.

(43) Patolsky, F.; Lichtenstein, A.; Willner, I. Detection of single-base DNA mutations by enzyme-amplified electronic transduction. *Nat. Biotechnol.* **2001**, *19*, 253–257.

(44) Cooper, M. A.; Dultsev, F. N.; Minson, T.; Ostanin, V. P.; Abell, C.; Klenerman, D. Direct and sensitive detection of a human virus by rupture event scanning. *Nat. Biotechnol.* **2001**, *19*, 833–837.

(45) Webster, A.; Vollmer, F.; Sato, Y. Probing biomechanical properties with a centrifugal force quartz crystal microbalance. *Nat. Commun.* **2014**, *5*, 5284.

(46) Suthar, J.; Parsons, E. S.; Hoogenboom, B. W.; Williams, G. R.; Guldin, S. Acoustic immunosensing of exosomes using a quartz crystal microbalance with dissipation monitoring. *Anal. Chem.* **2020**, *92*, 4082–4093.

(47) Richter, R. P.; Mukhopadhyay, A.; Brisson, A. Pathways of lipid vesicle deposition on solid surfaces: a combined QCM-D and AFM study. *Biophys. J.* **2003**, *85*, 3035–3047.

(48) Reimhult, E.; Larsson, C.; Kasemo, B.; Höök, F. Simultaneous surface plasmon resonance and quartz crystal microbalance with dissipation monitoring measurements of biomolecular adsorption events involving structural transformations and variations in coupled water. *Anal. Chem.* **2004**, *76*, 7211–7220.

(49) van der Meulen, S. A. J.; Dubacheva, G. V.; Dogterom, M.; Richter, R. P.; Leunissen, M. E. Quartz crystal microbalance with dissipation monitoring and spectroscopic ellipsometry measurements of the phospholipid bilayer anchoring stability and kinetics of hydrophobically modified DNA oligonucleotides. *Langmuir* **2014**, *30*, 6525–6533.

(50) Landau, L. D.; Lifshitz, E. M. *Fluid Mechanics*; Pergamon Press, 1987; Chapter II, pp 44–94.

(51) Perrault, S. D.; Chan, W. C. Synthesis and surface modification of highly monodispersed, spherical gold nanoparticles of 50–200 nm. *J. Am. Chem. Soc.* **2009**, *131*, 17042–17043.

(52) Johannsmann, D.; Reviakine, I.; Richter, R. P. Dissipation in films of adsorbed nanospheres studied by quartz crystal microbalance (QCM). *Anal. Chem.* **2009**, *81*, 8167–8176.

(53) Adamczyk, Z.; Sadowska, M. Hydrodynamic Solvent Coupling Effects in Quartz Crystal Microbalance Measurements of Nanoparticle Deposition Kinetics. *Anal. Chem.* **2020**, *92*, 3896–3903.

(54) Adamczyk, Z.; Sadowska, M.; Żeliszewska, P. Applicability of QCM-D for Quantitative Measurements of Nano- And Microparticle Deposition Kinetics: Theoretical Modeling and Experiments. *Anal. Chem.* **2020**, *92*, 15087–15095.

(55) Vázquez-Quesada, A.; Schofield, M. M.; Tsortos, A.; Mateos-Gil, P.; Milioni, D.; Gizeli, E.; Delgado-Buscalioni, R. Hydrodynamics of Quartz-Crystal-Microbalance DNA Sensors Based on Liposome Amplifiers. *Phys. Rev. Appl.* **2020**, *13*, 064059.

(56) Meléndez, M.; Vázquez-Quesada, A.; Delgado-Buscalioni, R. Load Impedance of Immersed Layers on the Quartz Crystal Microbalance: a Comparison with Colloidal Suspensions of Spheres. *Langmuir* **2020**, *36*, 9225–9234.

(57) Daikhin, L.; Gileadi, E.; Katz, G.; Tsionsky, V.; Urbakh, M.; Zagidulin, D. Influence of roughness on the admittance of the quartz crystal microbalance immersed in liquids. *Anal. Chem.* **2002**, *74*, 554–561.

(58) Armanious, A.; Aeppli, M.; Sander, M. Dissolved organic matter adsorption to model surfaces: adlayer formation, properties, and dynamics at the nanoscale. *Environ. Sci. Technol.* **2014**, *48*, 9420–9.

(59) Duval, J. F.; Wilkinson, K. I.; Van Leeuwen, H. P.; Buffle, J. Humic substances are soft and permeable: Evidence from their electrophoretic mobilities. *Environ. Sci. Technol.* **2005**, *39*, 6435–6445.

(60) Sutton, R.; Sposito, G. Molecular structure in soil humic substances: The new view. *Environ. Sci. Technol.* **2005**, *39*, 9009–9015.

(61) Armanious, A.; Aeppli, M.; Jacak, R.; Refardt, D.; Sigstam, T.; Kohn, T.; Sander, M. Viruses at solid-water interfaces: a systematic assessment of interactions driving adsorption. *Environ. Sci. Technol.* **2016**, *50*, 732–743.

(62) Klüpfel, L.; Piepenbrock, A.; Kappler, A.; Sander, M. Humic substances as fully regenerable electron acceptors in recurrently anoxic environments. *Nat. Geosci.* **2014**, *7*, 195–200.

(63) Latch, D. E.; McNeill, K. Microheterogeneity of singlet oxygen distributions in irradiated humic acid solutions. *Science* **2006**, *311*, 1743–1747.

(64) Ellis, J. S.; Thompson, M. Slip and coupling phenomena at the liquid-solid interface. *Phys. Chem. Chem. Phys.* **2004**, *6*, 4928–4938.

(65) Johannsmann, D.; Reviakine, I.; Rojas, E.; Gallego, M. Effect of sample heterogeneity on the interpretation of QCM(-D) data: comparison of combined quartz crystal microbalance/atomic force microscopy measurements with finite element method modeling. *Anal. Chem.* **2008**, *80*, 8891–8899.

(66) Friedt, J.-M.; Francis, L.; Choi, K.-H.; Frederix, F.; Campitelli, A. Combined atomic force microscope and acoustic wave devices: Application to electrodeposition. *J. Vac. Sci. Technol. A* **2003**, *21*, 1500–1505.

(67) Friedt, J.-M.; Choi, K. H.; Frederix, F.; Campitelli, A. Simultaneous AFM and QCM measurements: methodology validation using electrodeposition. *J. Electrochem. Soc.* **2003**, *150*, H229.

(68) Benkoski, J. J.; Höök, F. Lateral mobility of tethered vesicle-DNA assemblies. *J. Phys. Chem. B* **2005**, *109*, 9773–9779.

(69) Kučerka, N.; Tristram-Nagle, S.; Nagle, J. F. Structure of fully hydrated fluid phase lipid bilayers with monounsaturated chains. *J. Membr. Biol.* **2006**, *208*, 193–202.

(70) Rastogi, R. P.; Skukla, P. C.; Yadava, B. Membrane Permeability of Heavy Water. *Biochim. Biophys. Acta, Biomembr.* **1971**, *249*, 454–461.

(71) Roberts, K.; Alberts, B.; Johnson, A.; Walter, P.; Hunt, T. *Molecular Biology of the Cell*; Garland Science: New York, 2014; Chapter 11, pp 597–640.

(72) Bränden, M.; Tabaei, S. R.; Fischer, G.; Neutze, R.; Höök, F. Refractive-Index-Based Screening of Membrane-Protein Mediated Transfer Across Biological Membranes. *Biophys. J.* **2010**, *99*, 124–133.

(73) Daikhin, L.; Urbakh, M. Effect of surface film structure on the quartz crystal microbalance response in liquids. *Langmuir* **1996**, *12*, 6354–6360.

(74) Dolai, S.; Tabib-Azar, M. 433 MHz Lithium Niobate microbalance aptamer-coated whole Zika virus sensor with 370 Hz/ng sensitivity. *IEEE Sens. J.* **2020**, *20*, 4269–4274.